Journal of Statistical Mechanics: Theory and Experiment
An IOP and SISSA journal

A thermodynamically consistent non-ideal stochastic hard-sphere fluid

Aleksandar Donev[1,2], Berni J Alder[1] and Alejandro L Garcia[3]

[1] Lawrence Livermore National Laboratory, PO Box 808, Livermore, CA 94551-9900, USA
[2] Center for Computational Science and Engineering, Lawrence Berkeley National Laboratory, Berkeley, CA 94720, USA
[3] Department of Physics and Astronomy, San Jose State University, San Jose, CA 95192, USA
E-mail: aleks.donev@gmail.com, alder1@llnl.gov and algarcia@algarcia.org

Received 5 August 2009
Accepted 28 October 2009
Published 18 November 2009

Online at stacks.iop.org/JSTAT/2009/P11008
doi:10.1088/1742-5468/2009/11/P11008

Abstract. A grid-free variant of the direct simulation Monte Carlo (DSMC) method is proposed, named the isotropic DSMC (I-DSMC) method, that is suitable for simulating dense fluid flows at molecular scales. The I-DSMC algorithm eliminates all grid artifacts from the traditional DSMC algorithm; it is Galilean invariant and microscopically isotropic. The stochastic collision rules in I-DSMC are modified to yield a non-ideal structure factor that gives consistent compressibility, as first proposed by Donev *et al* (2008 *Phys. Rev. Lett.* **101** 075902). The resulting stochastic hard-sphere dynamics (SHSD) fluid is empirically found to have the same pair correlation function as a deterministic Hamiltonian system of penetrable spheres interacting with a linear core pair potential, well described by the hypernetted chain (HNC) approximation. We apply a stochastic Enskog kinetic theory to the SHSD fluid to obtain estimates for the transport coefficients that are in excellent agreement with particle simulations over a wide range of densities and collision rates. The fluctuating hydrodynamic behavior of the SHSD fluid is verified by comparing its dynamic structure factor against theory based on the Landau–Lifshitz Navier–Stokes equations. We also study the Brownian motion of a nanoparticle suspended in an SHSD fluid and find a long-time power-law tail in its velocity autocorrelation function consistent with hydrodynamic theory and molecular dynamics calculations.

1742-5468/09/P11008+25$30.00

Keywords: stochastic particle dynamics (theory), kinetic theory of gases and liquids, molecular dynamics, rarefied gas dynamics

ArXiv ePrint: 0908.0510

Contents

J. Stat. Mech. (2009) P11008

With the increased interest in nanofluidics and microfluidics, it has become necessary to develop tools for hydrodynamic calculations at the atomistic scale [1, 2]. There are several issues present for microscopic flows that are difficult to account for in models relying on the continuum Navier–Stokes equations. Firstly, it is complicated to deal with boundaries and interfaces in a way that consistently accounts for the bidirectional coupling between the flow and (moving) complex surfaces or suspended particles. Furthermore, it is not trivial to include thermal fluctuations in Navier–Stokes solvers [3]–[5], and in fact, most of the time the fluctuations are not included even though they can be very important at instabilities [6] or in driving the dynamics of suspended objects [7, 8]. Finally, since the grid cell sizes needed to resolve complex microscopic flows are small, a large computational effort is needed even for continuum solvers. An alternative is to use particle-based methods, which are explicit and unconditionally stable and rather simple to implement. The fluid particles are directly coupled to the microgeometry; for example, they directly interact with the beads of a polymer chain. Fluctuations occur naturally and the algorithm may be designed to give the correct spatio-temporal correlations.

Several particle methods have been described in the literature. The most accurate but also most expensive is molecular dynamics (MD) [9], and several coarse-grained

models have been developed, such as dissipative particle dynamics (DPD) [10] and multi-particle collision dynamics (MPCD) [11, 12], each of which has its own advantages and disadvantages [13]. Our method, first proposed in [14], is based on the direct simulation Monte Carlo (DSMC) algorithm of Bird [15]. The key idea behind DSMC is to replace deterministic interactions between the particles with stochastic momentum exchange (collisions) between nearby particles. While DSMC is usually viewed as a kinetic Monte Carlo algorithm for solving the Boltzmann equation for a low density gas, it can also be viewed as an alternative to the expensive MD in cases where an approximate (coarse-grained) treatment of the molecular transport is appropriate. The stochastic treatment of collisions makes the algorithm much simpler and faster than MD, while preserving the essential ingredients of fluctuating hydrodynamics: local momentum conservation, linear momentum exchange on length scales comparable to the particle size, and a similar fluctuation spectrum.

Being composed of point particles, the DSMC fluid has no internal structure, has an ideal gas equation of state (EOS), and is thus very compressible. As a consequence, the density fluctuations in DSMC are significantly larger than those in realistic liquids. Furthermore, the speed of sound is small (comparable to the average speed of the particles) and thus subsonic (Mach number less than 1) flows are limited to relatively small Reynolds numbers[4]. Efforts have been undertaken to develop coarse-grained models that have greater computational efficiency than brute-force MD and that have a *non-ideal* EOS, such as the lattice Boltzmann (LB) method [16], DPD [17], MPCD [18, 19]. The consistent Boltzmann algorithm (CBA) [20, 21], as well as algorithms based on the Enskog equation [22, 23], have demonstrated that DSMC fluids can have dense fluid compressibility; however, they did not achieve thermodynamic consistency between the equation of state and the fluid structure.

In this paper we describe a generalization of the traditional DSMC algorithm suitable for dense fluid flows. By a dense fluid we mean a fluid where the mean free path is small compared to the typical inter-atomic distance. As a first step, inspired by common practice in molecular dynamics, we introduce a grid-free *isotropic* DSMC (I-DSMC) method that eliminates all grid artifacts from traditional DSMC, notably the lack of Galilean invariance and non-isotropy. The I-DSMC fluid is still an *ideal* fluid just like the traditional DSMC fluid, that is, it has the equation of state of an ideal gas and does not have an internal structure as liquids do. Secondly, by biasing the collision kernel in I-DSMC to only allow stochastic collisions between approaching particles, we obtain a *stochastic hard-sphere dynamics* (SHSD) algorithm that is thermodynamically consistent (i.e., the direct calculation of compressibility from density fluctuations agrees with the density derivative of pressure). The SHSD algorithm is related to previous algorithms for solving the Enskog kinetic equation [22, 23], and can be viewed as a more efficient variable-diameter stochastic modification of the traditional hard-sphere molecular dynamics [24].

In the SHSD algorithm randomly chosen pairs of approaching particles that lie less than a given diameter from each other undergo collisions as if they were hard spheres of diameter equal to their actual separation. The SHSD fluid is shown to

[4] For a low density gas the Reynolds number is $Re \approx M/K$, where $M = v_{\text{flow}}/c$ is the Mach number, and the Knudsen number $K = \lambda/L$ is the ratio between the mean free path λ and the typical obstacle length L. This shows that subsonic flows can only achieve high Re flows for small Knudsen numbers, i.e., large numbers of DSMC particles.

J. Stat. Mech. (2009) P11008

be non-ideal, with pair correlations and an equation of state equivalent to that of a deterministic (Hamiltonian) fluid where penetrable spheres effectively interact with a repulsive linear core pairwise potential. We demonstrate this correspondence theoretically for low densities. Remarkably, we find numerically that this effective interaction potential, similar to the quadratic core potential used in many DPD variants, is valid at higher densities as well, and conjecture that the SHSD fluid has pairwise correlations that are identical to those of the linear core fluid. If our empirically supported conjecture is correct, the SHSD fluid, as in DPD, is *intrinsically* thermodynamically consistent since it satisfies the virial theorem.

The equivalence of the structure of the SHSD fluid with the linear core fluid enables us to use the hypernetted chain (HNC) approximation, as recommended in [25], to obtain theoretical estimates for the pair correlation and static structure factor that are in excellent agreement with numerical results. These further enable us to use the Enskog-like kinetic theory developed in [26] to obtain accurate theoretical estimates of the transport properties of the SHSD fluid that are also shown to be in excellent agreement with numerics even at relatively high densities. At lower densities the HNC approximation is not necessary and explicit expressions for the transport coefficients can be obtained similarly to what has been done using the Green–Kubo approach for other DSMC variants [20] and MPCD [13, 18, 27].

We numerically demonstrate that the hydrodynamics of the SHSD fluid is consistent with the equations of fluctuating hydrodynamics when the appropriate equation of state is taken into account. Specifically, we compare the measured dynamic structure factors with that obtained from the linearized fluctuating Navier–Stokes equations. We also calculate the velocity autocorrelation function (VACF) for a large hard spherical bead suspended in an SHSD fluid, demonstrating the existence of long-time tails as predicted by hydrodynamics and found in MD simulations. The tail is found to be in quantitative agreement with theory at lower densities, but a discrepancy is found at higher densities, possibly due to the strong structuring of the dense SHSD fluid.

We begin by introducing a grid-free variant of the DSMC algorithm in section 1. This isotropic DSMC algorithm simulates a stochastic particle system where particles closer than a particle diameter collide with a certain rate. By biasing the collision kernels to favor head-on collisions of particles, as in the hard-sphere fluid, we obtain a non-ideal stochastic fluid in section 2. We develop an Enskog-like kinetic theory for this stochastic hard-sphere dynamics (SHSD) system in section 2.1, which requires as input the pair correlation function. In section 2.2 we discover that the SHSD fluid is thermodynamically consistent with a fluid of penetrable linear core spheres, and use this equivalence to compute the pair correlation function of the SHSD fluid using the HNC approximation. In section 3 we show several numerical results, including a comparison with theory for the transport coefficients and for the dynamic structure factor, as well as a study of the hydrodynamic tails in the velocity autocorrelation of a bead suspended in an SHSD fluid.

1. Isotropic DSMC

The traditional DSMC algorithm [15, 28] starts with a time step where particles are propagated advectively, $\boldsymbol{r}_i' = \boldsymbol{r}_i + \boldsymbol{v}_i \Delta t$, and sorted into a grid of cells. Then, for each cell c a certain number $N_{\text{coll}} \sim \Gamma_{\text{sc}} N_{\text{c}}(N_{\text{c}} - 1)\Delta t$ of *stochastic collisions* are executed between

J. Stat. Mech. (2009) P11008

pairs of particles randomly chosen from the N_c particles inside the cell, where the collision rate Γ_{sc} is chosen on the basis of kinetic theory. The conservative stochastic collisions exchange momentum and energy between two particles i and j that is not correlated with the actual positions of the particles. Typically the probability of collision is made proportional to the magnitude of the relative velocity $v_r = |\boldsymbol{v}_{ij}|$ by using a conventional rejection procedure.

Traditional DSMC suffers from several grid artifacts, which become pronounced when the mean free path becomes comparable to the DSMC cell size. Firstly, the method is not Galilean invariant unless the grid of cells is shifted randomly before each collision step, as is typically done in the MPCD algorithm [11, 12] for the same reason. This shifting is trivial in a purely particle simulation with periodic boundary conditions, but it causes implementation difficulties when boundaries are present and also in particle–continuum hybrids [29]. Furthermore, traditional DSMC, unlike MD, is not microscopically isotropic and does not conserve angular momentum, leading to an anisotropic collisional stress tensor. Instead of trying to work around these grid artifacts, as is done for non-ideal MPCD in [18, 19], we have chosen to modify the traditional DSMC algorithm to make the dynamics grid-free.

To ensure isotropy, all particle pairs within a collision diameter D (i.e., *overlapping* particles if we consider the particles to be spheres of diameter D) are considered as potential collision partners even if they are in neighboring cells. In this way, the grid is only used as a tool for finding neighboring particles efficiently, but does not otherwise affect the properties of the resulting stochastic fluid, just as in molecular dynamics. Such a grid-free DSMC variant, which we will call the isotropic direct simulation Monte Carlo (I-DSMC) method, is suitable for studying the hydrodynamics of dense fluids, where the mean free path is comparable to or even smaller than D, unlike the original DSMC which targets the dilute limit. It is important to point out, however, that the I-DSMC is not meant to be a replacement for traditional DSMC for rarefied gas flows. In particular, the computational efficiency is reduced by a factor of 2–4 over traditional DSMC due to the need to search neighboring cells for collision partners in addition to the current cell. This added cost is not justified at low densities, where the grid artifacts of traditional DSMC are small. Furthermore, the I-DSMC method is not intended as a solver for the Boltzmann equation, which was the primary purpose of traditional DSMC [30, 31]. Rather, in the limit of small time steps, the I-DSMC method simulates the following *stochastic particle system*: particles move ballistically in between collisions. While two particles i and j are less than a diameter D apart, $r_{ij} \leq D$, there is a probability rate of $\chi D^{-1} K_c(\boldsymbol{v}_{ij}, \boldsymbol{r}_{ij})$ for them to collide and change velocities without changing their positions, where K_c is some function of the relative position and velocity of the pair, and the dimensionless *cross-section factor* χ sets the collisional frequency. Because the particles are penetrable, D and χ may be interpreted as the range and strength, respectively, of the interaction potential. After the collision, the pair center-of-mass velocity does not change, ensuring momentum conservation, while the relative velocity is drawn from a probability density $P_c(\boldsymbol{v}'_{ij}; \boldsymbol{v}_{ij}, \boldsymbol{r}_{ij})$, such that $\|\boldsymbol{v}'_{ij}\| = \|\boldsymbol{v}_{ij}\|$, so kinetic energy is conserved.

Once the *pre-collision and post-collision kernels* K_c and P_c are specified, the properties of the resulting I-DSMC fluid are determined by the cross-section factor χ and the *density* (hard-sphere volume fraction) $\phi = \pi N D^3/(6V)$, where N is the total number of particles in the simulation volume V. Compare this to the deterministic hard-sphere fluid, whose

J. Stat. Mech. (2009) P11008

properties are determined by the volume fraction ϕ alone. It is convenient to normalize the collision kernel K_c so that for an ideal gas with a Maxwell–Boltzmann velocity distribution the average collisional rate would be χ times larger than that of a gas of hard spheres of diameter D at low densities, $\phi \ll 1$. Two particular choices for the pre-collision kernel K_c that we use in practice are:

Traditional DSMC collisions (traditional I-DSMC ideal fluid), for which the probability of collision is made proportional to the magnitude of the relative velocity $v_{rel} = \|\boldsymbol{v}_{ij}\|$, $K_c = 3v_{rel}/4$. We use this kernel mainly for comparison with traditional DSMC.

Maxwell collisions (Maxwell I-DSMC ideal fluid), for which $K_c = 3\bar{v}_{rel}/4 = 3\sqrt{k_B T_0/\pi m}$, where $\bar{v}_{rel}$ is the average relative velocity at equilibrium temperature T_0. Since K_c is a constant, all pairs collide at the same rate, independently of their relative velocity. This kernel is not realistic and may lead to unphysical results in cases where there are large density and temperature gradients; however, it is computationally most efficient since there is no rejection based on relative velocity. We therefore prefer this kernel for problems where the temperature dependence of the transport properties is not important, and it is what we will typically mean when we say I-DSMC without further qualification.

Other collision kernels may be used in I-DSMC, though we will not consider them here [28]. We typically chose the traditional DSMC post-collisional kernel P_c in which the direction of the post-collisional relative velocity is randomized so as to mimic the average distribution of collision impact parameters in a low density hard-sphere gas. Specifically, in three dimensions the relative velocity is rotated uniformly independently of $\boldsymbol{r}_{ij}$ [15]. If one wishes to microscopically conserve angular momentum in I-DSMC then the post-collisional kernel has to use the actual positions of the colliding particles. Specifically, the component of the relative velocity perpendicular to the line joining the colliding particles should remain unchanged, while the parallel component should be reversed.

Note that a pairwise Anderson thermostat proposed within the context of MD/DPD by Lowe [32] adds I-DSMC-like collisions to ordinary MD. In addition to algorithmic differences with I-DSMC, in Lowe's method the post-collisional kernel is such that it preserves the normal component of the relative velocity (thus conserving angular momentum), while the parallel component is thermalized by drawing from a Maxwell–Boltzmann distribution. We strive to preserve exact conservation of both momentum and energy in the collision kernels that we use, without artificial energy transport via thermostating.

With a finite time step, the I-DSMC method can be viewed as a time-driven kinetic Monte Carlo algorithm for solving the master equation for the stochastic particle system described above. Unlike the singular kernel in the Boltzmann equation, this master equation has a mollified collision kernel with a finite compact support D [26, 33]. The traditional DSMC method also mollifies the collision kernel by considering particles within the same collision cell, of size L_c, as possible collision partners. This DSMC cell size is much larger than a molecular diameter, D_m, in fact, for low densities it is a fraction (typically a quarter) of the mean free path. The molecular properties enter in traditional DSMC only in the form of collisional cross-sections $\sigma \sim D_m^2$. In the light of this, for rarefied gas flows, the collision diameter D in I-DSMC should be considered the equivalent of the cell length L_c, and *not* D_m. Traditional DSMC is designed to reproduce a collision rate

J. Stat. Mech. (2009) P11008

per particle per unit time equal to the Boltzmann rate, $\Gamma_{\rm B}(D_{\rm m}) = CD_{\rm m}^2$, where C is a constant. The I-DSMC method is designed to reproduce a collision rate

$$\Gamma_{\rm I-DSMC} = \chi\Gamma_{\rm B}(D) = \chi CD^2,$$

and therefore by choosing

$$\chi = \chi_{\rm B} = \left(\frac{D_{\rm m}}{D}\right)^2$$

we get $\Gamma_{\rm I-DSMC} = \Gamma_{\rm B}(D_{\rm m})$. Therefore, if I-DSMC is used to simulate the transport in a low density gas of hard spheres of diameter $D_{\rm m}$, the collision diameter D should be chosen to be some fraction of the mean free path λ (say, $D \approx \lambda/4 \gg D_{\rm m}$), and the cross-section factor set to $\chi_{\rm B} \sim (D_{\rm m}/\lambda)^2 \ll 1$. At higher densities $\chi_{\rm B}$ starts becoming comparable to unity and thus it is no longer possible to separate the kinetic and collisional timescales as assumed in traditional DSMC. Note that I-DSMC is designed for dense fluids, so while it is possible to apply it in simulating rarefied gases it will not be as computationally efficient as traditional DSMC.

1.1. Performing stochastic collisions

In I-DSMC, stochastic collisions are processed at the beginning of every time step of duration Δt, and then each particle i is streamed advectively with constant velocity $\boldsymbol{v}_i$. During the collision step, we need to randomly and without bias choose pairs of overlapping particles for collision, given the current configuration of the system. This can be done, as in traditional DSMC, using a rejection Monte Carlo technique. Specifically, we need to choose a large number $N_{\rm tc}^{\rm (tot)} = \Gamma_{\rm tc}^{\rm (tot)} N_{\rm pairs}\Delta t$ of *trial collision pairs*, and then accept the fraction of them that are actually overlapping as *collision candidates*. Here $N_{\rm pairs}$ is the number of possibly overlapping pairs; for example, as a first guess one can include all pairs, $N_{\rm pairs} = N(N-1)/2$. The probability for choosing one of the overlapping pairs as a collision candidate is simply $\Gamma_{\rm tc}^{\rm (tot)}\Delta t$. If the probability of accepting a candidate pair ij for an actual collision is $p_{ij}^{\rm (acc)}$ and Δt is sufficiently small, then the probability *rate* of particles i and j actually colliding while they are overlapping approaches $\Gamma_{ij} = p_{ij}^{\rm (acc)}\Gamma_{\rm tc}^{\rm (tot)}$. The goal is to choose the trial collision frequency $\Gamma_{\rm tc}^{\rm (tot)}$ and $p_{ij}^{\rm (acc)}$ such that $\Gamma_{ij} = \chi D^{-1} K_{\rm c}(\boldsymbol{v}_{ij}, \boldsymbol{r}_{ij})$.

The efficiency of the algorithm is increased if the probability of accepting trial collisions is increased. In order to increase the acceptance probability, one should reduce $N_{\rm pairs}$ to be closer to the number of actually overlapping pairs; ideally, one would build a list of all the overlapping pairs (making $N_{\rm pairs}$ linear instead of quadratic in N). This is however expensive, and a reasonable compromise is to use collision cells, similarly to what is done in classical DSMC and also MD algorithms. Namely, the spatial domain of the simulation is divided into *cells* of length $L_{\rm c} \gtrapprox D$, and for each cell a linked list $\mathcal{L}_{\rm c}$ of all the particles in that cell is maintained. All pairs of particles that reside in the same or neighboring cells are considered as potential collision partners, and here we include the cell itself in its list of neighboring cells, i.e., each cell has 3^d neighbors, where d is the spatial dimension.

To avoid any spatial correlations (inhomogeneity and non-isotropy), trial collision pairs should be chosen at random, one by one. This would require first choosing a pair of

J. Stat. Mech. (2009) P11008

neighboring cells with the correct probability, and then choosing a particle from each cell (rejecting self-collisions). This is rather expensive to do, especially at lower χ, when few actual collisions occur at each time step, and we have therefore chosen to use a method that introduces a small bias each time step, but is unbiased over many time steps. Specifically, we visit the cells one by one and for each cell c we perform $N_{\mathrm{tc}}^{(c)} = \Gamma_{\mathrm{tc}}^{(c)} N_{\mathrm{c}} N_{\mathrm{p}} \Delta t$ trial collisions between one of the N_{c} particles in that cell and one of the N_{p} particles in the 3^d neighboring cells, rejecting self-collisions. Here $\Gamma_{\mathrm{tc}}^{(c)}$ is a *local* trial collision rate and it may depend on the particular cell c under consideration. Note that each of the $N_{\mathrm{c}}(N_{\mathrm{c}}-1)$ trial pairs ij where both i and j are in cell c is counted twice, and similarly, any pair where i and j are in different cells c and c' is included as a trial pair twice, once when each of the cells c and c' is considered. Also note that it is important not to visit the cells in a fixed order during every time step. Unlike in traditional cells, where cells are independent of each other and can be visited in an arbitrary order (even in parallel), in I-DSMC it is necessary to ensure isotropy by visiting the cells in a random order, which is different every time step.

For the Maxwell pre-collision kernel, once a pair of overlapping particles i and j is found, a collision is performed without additional rejection; therefore, we set $\Gamma_{\mathrm{tc}}^{(c)} = \chi D^{-1} K_{\mathrm{c}}/2 = 3\chi(2D)^{-1}\sqrt{k_{\mathrm{B}}T_0/\pi m} = \text{const}$. Note that we have divided by 2 because of the double counting of each trial pair. For the traditional pre-collision kernel, and, as we shall see shortly, the SHSD pre-collision kernel, additional rejection based on the relative velocity $\boldsymbol{v}_{ij}$ is necessary. As in the traditional DSMC algorithm, we estimate an upper bound for the maximal value of the pre-collision kernel $K_{\mathrm{c}}^{(\max)}$ among the pairs under consideration and set $\Gamma_{\mathrm{tc}}^{(c)} = \chi D^{-1} K_{\mathrm{c}}^{(\max)}/2$. We then perform an actual collision for the trial pair ij with probability

$$p_{ij}^{c} = K_{\mathrm{c}}(\boldsymbol{v}_{ij}, \boldsymbol{r}_{ij})/K_{\mathrm{c}}^{(\max)},$$

giving the correct collision probability for every overlapping pair of particles. For the traditional pre-collision kernel $K_{\mathrm{c}}^{(\max)} = 3v_{\mathrm{rel}}^{(\max)}/4$, where $v_{\mathrm{rel}}^{(\max)}$ is as tight an estimate of the maximum relative speed as possible. In the traditional DSMC algorithm, $v_{\mathrm{rel}}^{(\max)}$ is a global bound obtained by simply keeping track of the maximum particle speed $v_{\max}$ and taking $v_{\mathrm{rel}}^{(\max)} = 2v_{\max}$ [15]. In I-DSMC, we obtain a local estimate of $v_{\mathrm{rel}}^{(\max)}$ for each cell c that is visited, thus increasing the acceptance rate and improving efficiency.

Algorithm 1 specifies the procedure for performing collisions in the I-DSMC method. The algorithm is to a large degree collision kernel independent, and in particular, the same algorithm is used for ideal and non-ideal stochastic fluids. As already explained, the size of the cells should be chosen to be as close as possible to but still larger than the particle diameter D. The time step should be chosen such that a typical particle travels a distance $l_{\Delta t} \approx v_{\mathrm{th}}\Delta t \sim D\delta t$, where the typical thermal velocity $v_{\mathrm{th}} = \sqrt{k_{\mathrm{B}}T_0/m}$ and δt is a dimensionless time step, which should be kept reasonably smaller than 1; for example, $\delta t \lessapprox 0.25$. It is also important to ensure that each particle does not, on average, undergo more than one collision per time step; we usually keep the number of collisions per particle per time step less than 1/2. Since a typical value of the pre-collision kernel is $K_{\mathrm{c}} \sim v_{\mathrm{th}}$, the number of collisions per particle per time step can easily be seen to be of the order of

$$N_{\mathrm{cps}} \sim \chi \frac{v_{\mathrm{th}}}{D} \frac{N}{V} V_{\mathrm{p}} \Delta t = \chi \phi \delta t,$$

J. Stat. Mech. (2009) P11008

where $V_\mathrm{p} \sim D^3$ is a particle volume. Therefore, unless $\chi\phi \gg 1$, choosing a small dimensionless time step δt will ensure that the collisional frequency is not too large, $N_\mathrm{cps} \ll 1$. With these conditions observed, we find little dependence of the fluid properties on the actual value of δt.

Algorithm 1: Processing of stochastic collisions between overlapping particles at a time step in the I-DSMC method.

1. Sample a random permutation of the cell numbering $\mathcal{P}$.

2. Visit the cells one by one in the random order given by $\mathcal{P}$. For each cell c, do the following steps if the number of particles in that cell $N_\mathrm{c} > 0$; otherwise move on to the next cell.

3. Build a list $\mathcal{L}_1$ of the N_c particles in the cell and at the same time find the largest particle speed in that cell, v_1^max. Also keep track of the second-largest speed in that cell, v_2^max, which is an estimate of the largest possible speed of a collision partner for the particle with speed v_1^max.

4. Build a list of the N_p particles in the set of 3^d cells that neighbor c, including the cell c itself and respecting the proper boundary conditions. Also update v_2^max if any of the potential collision partners not in cell c have speeds greater than v_2^max.

5. Determine the number of trial collisions between a particle in cell c and a neighboring particle by rounding to an integer [15] the expected value

$$N_\mathrm{tc} = \Gamma_\mathrm{tc} N_\mathrm{c} N_\mathrm{p} \Delta t,$$

where Δt is the time step. Here the local trial collision rate is

$$\Gamma_\mathrm{tc} = \frac{\chi K_\mathrm{c}^\mathrm{max}}{2D},$$

where $K_\mathrm{c}^\mathrm{max}$ is an upper bound for the pre-collision kernel among all candidate pairs. For Maxwell collisions $K_\mathrm{c}^\mathrm{max} = 3\sqrt{k_\mathrm{B}T_0/\pi m}$, and for traditional collisions $K_\mathrm{c}^\mathrm{max} = 3v_\mathrm{rel}^\mathrm{(max)}/4$, where $v_\mathrm{max}^\mathrm{(rel)} = (v_1^\mathrm{max} + v_2^\mathrm{max})$ is a local upper bound on the relative speed of a colliding pair.

6. Perform trial collisions by randomly selecting N_tc pairs of particles $i \in \mathcal{L}_1$ and $j \in \mathcal{L}_2$. For each pair, do the following steps if $i \neq j$:

   (a) Calculate the distance l_{ij} between the centroids of particles i and j, and go to the next pair if $l_{ij} > D$.
   (b) Calculate the collision kernel $K_{ij}^c = K_\mathrm{c}(\boldsymbol{v}_{ij}, \boldsymbol{r}_{ij})$, and go to the next pair if $K_{ij}^c = 0$.
   (c) Sample a random uniform variate $0 < r \leq 1$ and go to the next pair if $K_{ij}^c \leq rK_\mathrm{c}^\mathrm{max}$ (note that this step can be skipped in Maxwell I-DSMC since $K_{ij}^c = K_\mathrm{c}^\mathrm{max}$).
   (d) Process a stochastic collision between the two particles by updating the particle velocities by sampling the post-collision kernel $P_\mathrm{c}(\boldsymbol{v}'_{ij}; \boldsymbol{v}_{ij}, \boldsymbol{r}_{ij})$. For ideal fluids we perform the usual stochastic DSMC collision by randomly rotating $\boldsymbol{v}_{ij}$ to obtain $\boldsymbol{v}'_{ij}$, independently of $\boldsymbol{r}_{ij}$.

J. Stat. Mech. (2009) P11008

2. Stochastic hard-sphere dynamics

The traditional DSMC fluid has no internal structure so it has an ideal gas equation of state (EOS), $p = PV/Nk_BT = 1$, and is thus very compressible. As for the classical hard-sphere fluid, the pressure of fluids with stochastic collisions consists of two parts: the usual *kinetic* contribution that gives the ideal gas pressure $p_k = 1$, and a *collisional* contribution proportional to the virial $p_c \sim \langle (\boldsymbol{v}_{ij} \cdot \boldsymbol{r}_{ij})' - (\boldsymbol{v}_{ij} \cdot \boldsymbol{r}_{ij}) \rangle_c$, where the average is over stochastic collisions and primes denote post-collisional values. The virial vanishes for collision kernels where velocity updates and positions are uncorrelated, as in traditional DSMC, leaving only the ideal gas kinetic contribution. In order to introduce a non-trivial equation of state it is necessary to either give an additional displacement $\Delta \boldsymbol{r}_{ij}$ to the particles that is parallel to $\boldsymbol{v}_{ij}$, or to bias the momentum exchange $\Delta \boldsymbol{p}_{ij} = m \Delta \boldsymbol{v}_{ij}$ to be (statistically) aligned to $\boldsymbol{r}_{ij}$. The former approach has already been investigated in the consistent Boltzmann algorithm (CBA) [20, 21]. This algorithm was named 'consistent' because both the transport coefficients and the equation of state are consistent with those of a hard-sphere fluid to lowest order in density, unlike traditional DSMC which only matches the transport coefficients. However, CBA is not *thermodynamically* consistent since it modifies the compressibility without affecting the density fluctuations (i.e., the structure of the fluid is still that of a perfect gas).

Here we explore the option of biasing the stochastic momentum exchange on the basis of the position of the colliding particles. What we are trying to emulate through this bias is an effective repulsion between overlapping particles. This repulsion will be maximized if we make $\Delta \boldsymbol{p}_{ij}$ parallel to $\boldsymbol{r}_{ij}$, that is, if we use the hard-sphere collision rule $P_c(\boldsymbol{v}'_{ij}; \boldsymbol{v}_{ij}, \boldsymbol{r}_{ij}) = \delta(\boldsymbol{v}_{ij} + 2v_n \hat{\boldsymbol{r}}_{ij})$, where $v_n = -\boldsymbol{v}_{ij} \cdot \hat{\boldsymbol{r}}_{ij}$ is the normal component of the relative velocity. Explicitly, we have particles collide as if they are elastic hard spheres of diameter equal to the distance between them at the time of the collision,

$$\begin{aligned} \boldsymbol{v}'_i &= \boldsymbol{v}_i + v_n \hat{\boldsymbol{r}}_{ij} \\ \boldsymbol{v}'_j &= \boldsymbol{v}_j - v_n \hat{\boldsymbol{r}}_{ij}. \end{aligned} \tag{1}$$

Such collisions produce a positive virial only if the particles are approaching each other, i.e., if $v_n > 0$; therefore, we reject collisions among particles that are moving apart, $K_c(\boldsymbol{v}_{ij}, \boldsymbol{r}_{ij}) \sim \Theta(v_n)$, where Θ denotes the Heaviside function. Note that the hard-sphere post-collision rule (1) strictly conserves angular momentum in addition to linear momentum and energy and can be used with other pre-collision kernels (e.g., Maxwell) if one wishes to conserve angular momentum.

To avoid rejection of candidate collision pairs and thus make the algorithm most efficient, it would be best if the pre-collision kernel K_c is independent of the relative velocity as for Maxwell collisions. However, without rejection based on the normal v_n or relative v_r speeds, fluctuations of the local temperature T_c would not be consistently coupled to the local pressure. Namely, without rejection the *local* collisional frequency Γ_{sc} would be independent of T_c and thus the collisional contribution to the pressure $p_c \sim \langle \Delta \boldsymbol{v}_{ij} \cdot \boldsymbol{r}_{ij} \rangle_c \sim \Gamma_{sc} \sqrt{T_c}$ would be $p_c \sim \sqrt{T_c}$ instead of $p_c \sim T_c$, as is required for a fluid with no internal energy [18, 19]. Instead, as for hard spheres, we require that $\Gamma_{sc} \sim \sqrt{T_c}$, which is satisfied if the collision kernel is linear in the magnitude of the relative velocity. For DSMC the collisional rules can be manipulated arbitrarily to obtain the desired transport coefficients; however, for non-ideal fluids thermodynamic requirements eliminate

J. Stat. Mech. (2009) P11008

some of the freedom. This important observation has not been taken into account in other algorithms that randomize hard-sphere molecular dynamics [34], but has been used in the non-ideal MPCD algorithm in order to obtain thermodynamic consistency [18, 19].

There are two obvious choices for a pre-collision kernel that are linear in the magnitude of the relative velocity. One is to use the relative speed, $K_c \sim v_r$, as in the traditional DSMC algorithm, and the other is to use the hard-sphere pre-collision kernel, $K_c \sim v_n$. We have chosen to make the collision probability linear in the normal speed v_n; specifically, we take $K_c = 3v_n\Theta(v_n)$ to define the *stochastic hard-sphere dynamics* (SHSD) fluid, like what has previously been done in the Enskog DSMC algorithm [22, 23] and in non-ideal MPCD [18, 19]. These choices for the collision kernels make the SHSD fluid identical to the one proposed in [33] for the purposes of proving convergence of a microscopic model to the Navier–Stokes equations. Specifically, the singular Boltzmann hard-sphere collision kernel is mollified in [33] to obtain the SHSD collision kernel and then the low density hydrodynamic limit is considered.

The non-ideal SHSD fluid is simulated by the I-DSMC method, in the limit of sufficiently small time steps. However, it is important to observe that the SHSD fluid is defined independently of any temporal discretization used in computer simulations, just like a Hamiltonian fluid is defined through the equations of motion independently of molecular dynamics (MD). To summarize, in the SHSD algorithm we use the following collision kernels in algorithm 1:

$$K_c = 3v_n\Theta(v_n) \qquad \text{and} \qquad K_c^{(\max)} = 3v_{\max}^{(\mathrm{rel})}$$
$$P_c(\boldsymbol{v}'_{ij}) = \delta(\boldsymbol{v}_{ij} + 2v_n\hat{\boldsymbol{r}}_{ij})$$
$$\text{where } v_n = -\boldsymbol{v}_{ij}\cdot\hat{\boldsymbol{r}}_{ij}.$$

Note that considering particles in neighboring cells as collision partners is essential in SHSD in order to ensure isotropy of the collisional (non-ideal) component of the pressure tensor. It is also important to traverse the cells in random order when processing collisions, as well as to ensure a sufficiently small time step is used to faithfully simulate the SHSD fluid. Note that the SHSD algorithm strictly conserves both momentum and energy independently of the time step.

2.1. Enskog kinetic theory

In this section we develop some kinetic equations for the SHSD fluid that are inspired by the Enskog theory of hard-sphere fluids. Remarkably, it turns out that these sorts of kinetic equations have already been studied in the literature for purely theoretical purposes.

2.1.1. BBGKY hierarchy. The full Bogoliubov–Born–Green–Kirkwood–Yvon (BBGKY) hierarchy of master equations describing the SHSD fluid is derived in [33]. Specifically, the evolution of the s-particle distribution function $f_s(t;\boldsymbol{r}_1,\boldsymbol{v}_1,\ldots,\boldsymbol{r}_s,\boldsymbol{v}_s)$ is governed by

$$\frac{\partial f_s}{\partial t} + \sum_{i=1}^{s}\boldsymbol{v}_i\cdot\boldsymbol{\nabla}_{\boldsymbol{r}_i}f_s = 3\chi D^2\int_0^1 \mathrm{d}x\int_{\mathcal{R}^3}\mathrm{d}\boldsymbol{v}_j\int_{S_+^2}\mathrm{d}\hat{\boldsymbol{r}}_{ij}\,x^2\sum_{i=1}^{s}v_n$$
$$\times\,[f_{s+1}(t;\boldsymbol{r}_1,\boldsymbol{v}_1,\ldots,\boldsymbol{r}_i,\boldsymbol{v}'_i,\ldots,\boldsymbol{r}_s,\boldsymbol{v}_s,\boldsymbol{r}_i+x\hat{\boldsymbol{r}}_{ij},\boldsymbol{v}'_j)$$
$$-\,f_{s+1}(t;\boldsymbol{r}_1,\boldsymbol{v}_1,\ldots,\boldsymbol{r}_i,\boldsymbol{v}_i,\ldots,\boldsymbol{r}_s,\boldsymbol{v}_s,\boldsymbol{r}_i-x\hat{\boldsymbol{r}}_{ij},\boldsymbol{v}_j)] \qquad (2)$$

J. Stat. Mech. (2009) P11008

which takes into account the contribution from collisions of one of the s particles, particle i, with another particle j that is at a distance $r_{ij} = xD$ away, $0 \le x \le 1$. Here S_+^2 denotes the fraction of the unit sphere for which $v_n = -\hat{\boldsymbol{r}}_{ij} \cdot (\boldsymbol{v}_i - \boldsymbol{v}_j) \ge 0$, and $\boldsymbol{v}_i' = \boldsymbol{v}_i + v_n \hat{\boldsymbol{r}}_{ij}$ and $\boldsymbol{v}_j' = \boldsymbol{v}_j - v_n \hat{\boldsymbol{r}}_{ij}$. Just like the BBGKY hierarchy for Hamiltonian fluids, equations (2) are exact; however, they form an infinite unclosed system in which the $(s+1)$-particle distribution function appears in the equation for the s-particle distribution function. As usual, we need to make an ansatz to truncate and close the system, as we do next.

2.1.2. Thermodynamic and transport properties. The hydrodynamics of the SHSD fluid is well described by a kinetic equation for the single-particle probability distribution $f(t, \boldsymbol{r}, \boldsymbol{v}) \equiv f_1(t; \boldsymbol{r}, \boldsymbol{v})$ obtained by making the common molecular chaos assumption about the two-particle distribution function,

$$f_2(t; \boldsymbol{r}_1, \boldsymbol{v}_1, \boldsymbol{r}_2, \boldsymbol{v}_2) = g_2(\boldsymbol{r}_1, \boldsymbol{r}_2; n) f(t, \boldsymbol{r}_1, \boldsymbol{v}_1) f(t, \boldsymbol{r}_2, \boldsymbol{v}_2),$$

where $g_2(\boldsymbol{r}_i, \boldsymbol{r}_j; n)$ is the non-equilibrium pair distribution function that is a functional of the local number density $n(\boldsymbol{r})$. At global equilibrium $n(\boldsymbol{r}) = \text{const}$, and $g_2 \equiv g_2(r_{ij})$ depends only on the radial distance once the equilibrium density n and cross-section factor χ are specified. Substituting the above assumption for f_2 in the first equation of the BBGKY hierarchy (2), we get a stochastic revised Enskog equation of the form studied in [26],

$$\begin{aligned}\frac{\partial f(t, \boldsymbol{r}, \boldsymbol{v})}{\partial t} + \boldsymbol{v} \cdot \boldsymbol{\nabla}_{\boldsymbol{r}} f(t, \boldsymbol{r}, \boldsymbol{v}) = 3\chi D^2 \int_0^1 \mathrm{d}x \int_{\mathcal{R}^3} \mathrm{d}\boldsymbol{w} \int_{S_+^2} \mathrm{d}\boldsymbol{e}\, x^2 v_n \\ \times \left[g_2(\boldsymbol{r}, \boldsymbol{r} + x\boldsymbol{e}; n) f(t, \boldsymbol{r}, \boldsymbol{v}') f(t, \boldsymbol{r} + x\boldsymbol{e}, \boldsymbol{w}') \right. \\ \left. - g_2(\boldsymbol{r}, \boldsymbol{r} - x\boldsymbol{e}; n) f(t, \boldsymbol{r}, \boldsymbol{v}) f(t, \boldsymbol{r} - x\boldsymbol{e}, \boldsymbol{w}) \right] \end{aligned} \tag{3}$$

where $v_n = -\boldsymbol{e} \cdot (\boldsymbol{v} - \boldsymbol{w}) \ge 0$, $\boldsymbol{v}' = \boldsymbol{v} + \boldsymbol{e} v_n$ and $\boldsymbol{w}' = \boldsymbol{w} - \boldsymbol{e} v_n$.

The standard second-order Chapman–Enskog expansion has been carried out for the 'stochastic Enskog' equation of the same form as equation (3) in [26], giving the equation of state (EOS) $p = PV/Nk_{\mathrm{B}}T$, and estimates of the diffusion coefficient ζ, the shear η and bulk η_{B} viscosities, and thermal conductivity κ of the SHSD fluid. The expressions in [26] ultimately express the transport coefficients in terms of various dimensionless integer moments of the pair correlation function $g_2(x = r/D)$, $x_k = \int_0^1 x^k g_2(x)\, \mathrm{d}x$, specifically,

$$p - 1 = 12\phi\chi x_3, \tag{4}$$

$$\zeta/\zeta_0 = \frac{\sqrt{\pi}}{48\phi\chi x_2}, \tag{5}$$

$$\eta_{\mathrm{B}}/\eta_0 = \frac{48\phi^2\chi x_4}{\pi^{3/2}}, \tag{6}$$

$$\eta/\eta_0 = \frac{5}{48\sqrt{\pi}\chi x_2}\left(1 + \frac{24\phi\chi x_3}{5}\right)^2 + \frac{3}{5}\eta_{\mathrm{B}}, \qquad \text{and} \tag{7}$$

$$\kappa/\kappa_0 = \frac{25}{64\sqrt{\pi}\chi x_2}\left(1 + \frac{36\phi\chi x_3}{5}\right)^2 + \frac{3}{2}\eta_{\mathrm{B}}, \tag{8}$$

J. Stat. Mech. (2009) P11008

where $\zeta_0 = D\sqrt{k_\mathrm{B}T/m}$, $\eta_0 = D^{-2}\sqrt{mk_\mathrm{B}T}$ and $\kappa_0 = k_\mathrm{B}D^{-2}\sqrt{k_\mathrm{B}T/m}$ are natural units. These equations are very similar to the ones in the Enskog theory of the hard-sphere fluid except that various coefficients are replaced with moments of $g_2(x)$. In order to use these equations, however, we need to have a good approximation to the pair correlation function, i.e., to the structure of the SHSD fluid. It is important to point out that equation (4) is *exact*, as it can be derived directly from the definition of the collisional contribution to the pressure.

2.2. Pair correlation function

In this section we study the structure of the SHSD fluid, theoretically at low densities, and then numerically at higher densities. We find, surprisingly, that there is a thermodynamic correspondence between the stochastic SHSD fluid and a deterministic penetrable sphere fluid.

2.2.1. Low densities. In order to understand properties of the SHSD fluid as a function of the density ϕ and the cross-section factor χ, we first consider the equilibrium pair correlation function $g_2(r)$ at low densities, where correlations higher than pairwise can be ignored. We consider the cloud of point walkers ij representing the $N(N-1)/2$ pairs of particles, each at position $\boldsymbol{r} = \boldsymbol{r}_i - \boldsymbol{r}_j$ and with velocity $\boldsymbol{v} = \boldsymbol{v}_i - \boldsymbol{v}_j$. If one of these walkers is closer than D to the origin, $r \le D$, and is approaching the origin, $v_n > 0$, it reverses its radial speed as a stochastic process with a time-dependent rate $\Gamma = |v_n|\Gamma_0$, where $\Gamma_0 = 3\chi/D$ is the collision frequency. A given walker corresponding to pair ij also undergoes stochastic spatially unbiased velocity changes with some rate due to the collisions of i with other particles. At low densities we can assume that these additional collisions merely thermalize the velocities to a Maxwell–Boltzmann distribution but do not otherwise couple with the radial dependence of the one-particle distribution function $f_\mathrm{pairs}(\boldsymbol{v},\boldsymbol{r})$ of the $N(N-1)/2$ walkers. Inside the core $r \le D$ this distribution of pair walkers satisfies a kinetic equation

$$\frac{\partial f_\mathrm{pairs}}{\partial t} - v_n\frac{\partial f_\mathrm{pairs}}{\partial r} = \begin{cases} -\Gamma f_\mathrm{pairs} & \text{if } v_n \ge 0 \\ \Gamma f_\mathrm{pairs} & \text{if } v_n < 0 \end{cases} = -\Gamma_0 v_n f_\mathrm{pairs}, \tag{9}$$

where the term $-\Gamma f_\mathrm{pairs}$ is a loss term for approaching pairs due to their collisions, while Γf_pairs is a gain term for pairs that are moving apart due to collisions of approaching pairs that then reverse their radial speed. At equilibrium, $\partial f_\mathrm{pairs}/\partial t = 0$, and v_n cancels on both sides, consistently with choosing collision probability linear in $|v_n|$, giving $\partial f_\mathrm{pairs}/\partial r = 3\chi D^{-1} f_\mathrm{pairs}$. At equilibrium, the distribution of the point walkers in phase space ought to be of the separable form $f_\mathrm{pairs}(\boldsymbol{v},\boldsymbol{r}) = f_\mathrm{pairs}(v_n, r) \sim g_2(r)\exp(-mv_n^2/4kT)$, giving $\mathrm{d}g_2(r)/\mathrm{d}r = 3\chi D^{-1} g_2(r)$ for $r \le D$ and zero otherwise, with the solution

$$g_2(x = r/D) = \begin{cases} \exp[3\chi(x-1)] & \text{for } x \le 1 \\ 1 & \text{for } x > 1. \end{cases} \tag{10}$$

Indeed, numerical experiments confirmed that at sufficiently low densities the equilibrium g_2 for the SHSD fluid has the exponential form (10) inside the collision core. From statistical mechanics we know that for a deterministic Hamiltonian particle system

J. Stat. Mech. (2009) P11008

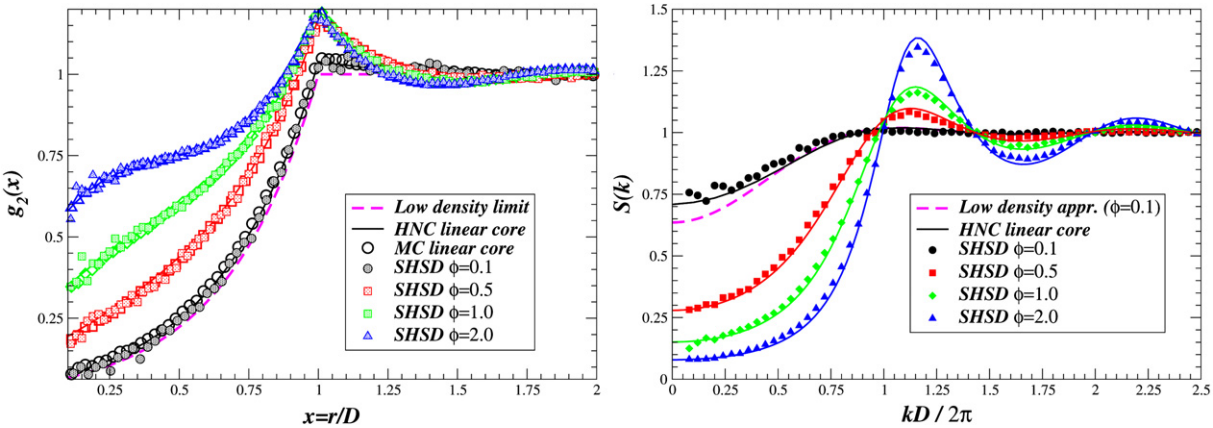

Figure 1. (*Left.*) The equilibrium pair correlation function of the SHSD fluid (solid symbols, $N = 10^4$ particles in a cubic periodic box), compared to Monte Carlo simulations (open symbols, $N = 10^4$ particles in a cubic periodic box) and numerical solution of the HNC equations (solid lines) for the linear core system, at various densities and $\chi = 1$. The low density approximation corresponding to equation (10) is also shown. (*Right.*) The corresponding static structure factors from SHSD simulations (solid symbols, averages of ten snapshots of a system with $N = 10^5$ particles in a cubic periodic box) and HNC calculations (solid lines). The time step was kept sufficiently small in the SHSD simulations to ensure that the results faithfully represent the SHSD fluid with time step errors smaller than the statistical uncertainties, which are of the order of the largest symbol size except at the smallest x where there is less sampling.

with a pairwise potential $U(r)$ at low density, $g_2^U = \exp[-U(r)/kT]$. Therefore, the low density result (10) is consistent with an effective *linear core* pair potential

$$U_{\text{eff}}(r)/kT = 3\chi(1-x)\Theta(1-x). \tag{11}$$

Note that this repulsive potential is similar to the quadratic core potential used in DPD and strictly vanishes outside of the overlap region, as expected. Also note that the cross-section factor χ plays the role that $U(0)/kT$ plays in the system of penetrable spheres interacting with a linear core pairwise potential.

As pointed out earlier, equation (4) is exact. At the same time, it is equivalent to the virial theorem for the linear core potential. Therefore, if the pair correlation functions of the SHSD fluid and the linear core fluid are truly identical, the pressure of the SHSD fluid is identically equal to that of the corresponding penetrable sphere system. As a consequence, the thermodynamic consistency between the structure ($g_2(x)$ and $S(k)$) and equation of state ($p(\phi)$) is guaranteed to be exact for the SHSD fluid.

2.2.2. Equivalence to the linear core penetrable sphere system. Remarkably, we find *numerically* that the effective potential (11) can predict $g_2(x)$ exactly, at *all* densities. In fact, we have numerically observed that the SHSD fluid behaves thermodynamically *identically* to a system of penetrable spheres interacting with a linear core pairwise potential for all ϕ and χ that we have tried, including densities at which freezing is observed. Figure 1 shows a comparison between the pair correlation function of the SHSD

J. Stat. Mech. (2009) P11008

fluid on one hand, and a Monte Carlo calculation using the linear core pair potential on the other, at several densities. Also shown is a numerical solution to the hypernetted chain (HNC) integral equations for the linear core system, inspired by its success for the Gaussian core model [25]. The excellent agreement at all densities permits the use of the HNC result in practical applications, notably the calculation of the transport coefficients via the Enskog-like kinetic theory presented in section 2.1.2. We also show the static structure factor $S(k)$ in figure 1, and find very good agreement between numerical results and the HNC theory, as expected since $S(k)$ can be expressed as the Fourier transform of $h(r) = g_2(r) - 1$. We have not examined correlations of order higher than pairwise in detail, since the pressure and transport coefficient estimates that we use depend only on the pair correlation function.

For collision frequencies $\chi \lesssim 1$ the structure of the SHSD fluid is quite different from that of the hard-sphere fluid because the particles inter-penetrate and overlap significantly. Interestingly, in the limit of infinite collision frequency $\chi \to \infty$ the SHSD fluid reduces to the hard-sphere (HS) fluid for sufficiently low densities. In fact, if the density ϕ is smaller than the freezing point for the HS system, the structure of the SHSD fluid approaches, as χ increases, that of the HS fluid. For higher densities, if χ is sufficiently high, crystallization is observed in SHSD, either to the usual hard-sphere crystals if ϕ is lower than the close-packing density, or if not, to an unusual partially ordered state with multiple occupancy per site, typical of weakly repulsive potentials [35]. Monte Carlo simulations of the linear core penetrable sphere system show identical freezing behavior to SHSD, confirming the surprising equivalence even at non-fluid densities. This points to a conjecture that the (unique) stationary solution to the BBGKY hierarchy (2) is the equilibrium Gibbs distribution,

$$f_s^E = \frac{\prod_{i=1}^{s} M(\boldsymbol{v}_i)}{Z_N} \int_{\boldsymbol{r}_{s+1}} \cdots \int_{\boldsymbol{r}_N} \exp\left[-\beta \sum_{i<j} U_{\text{eff}}(r_{ij})\right] \mathrm{d}\boldsymbol{r}_{s+1} \cdots \mathrm{d}\boldsymbol{r}_N,$$

where M is a Maxwellian. Further numerical tests of this conjecture could be obtained by performing a detailed comparison of higher order correlation functions and phase diagrams of the two fluids. However, the unexpected relation between the pair correlation functions of the two fluids, demonstrated above, is sufficient to enable us to apply well-established liquid state and kinetic theories to the SHSD fluid.

3. Results

In this section we perform several numerical experiments with the SHSD algorithm. Firstly, we compare the theoretical predictions for the transport properties of the SHSD fluid on the basis of the HNC theory for the linear core penetrable sphere system with results from particle simulations. We then compute dynamic structure factors and compare them to predictions of fluctuating hydrodynamics. Finally, we study the motion of a Brownian bead suspended in an SHSD fluid.

3.1. Thermodynamic and transport properties

The equation of state of the SHSD fluid for a given χ is $P = p(\phi)Nk_{\mathrm{B}}T/V$, where $p(\phi)$ is given in equation (4). According to statistical mechanics, the structure factor at the

J. Stat. Mech. (2009) P11008

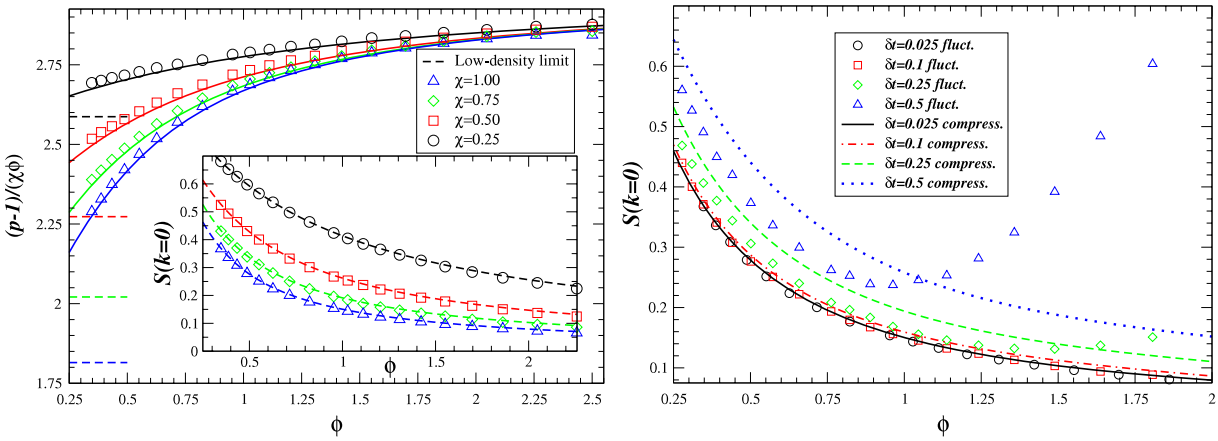

Figure 2. (*Left.*) The normalized equation of state $(p-1)/(\chi\phi)$ for the SHSD fluid at several cross-section factors χ (different symbols, $N = 10^5$ particles in a cubic box) compared to theoretical predictions based on the virial theorem (4) with the HNC approximation to $g_2(x)$ (solid lines). The inset compares the compressibility $(p + \phi\,\mathrm{d}p/\mathrm{d}\phi)^{-1}$ (dashed lines) to the structure factor at the origin $S(k \to 0)$ (symbols), measured using a direct Fourier transform of the particle positions for small k and extrapolating to $k = 0$. The dimensionless time step $\delta t = 0.025$ is kept constant and small as the density is changed. (*Right.*) Thermodynamic consistency between the compressibility (lines) and the large-scale density fluctuations $S(k \to 0)$ (symbols) for different dimensionless time steps δt, keeping $\chi = 1$ fixed.

origin is equal to the isothermal compressibility, that is,

$$S_0 = S(\omega = 0, k = 0) = \tilde{c}_T^{-2} = (p + \phi\,\mathrm{d}p/\mathrm{d}\phi)^{-1}$$

where $c_T = \tilde{c}_T\sqrt{k_\mathrm{B}T/m}$ is the isothermal speed of sound. In the inset in the top part of figure 2, we directly demonstrate the thermodynamic consistency of SHSD by comparing the compressibility calculated through numerical differentiation of the pressure to the structure factor at the origin. The pressure is easily measured in the particle simulations by keeping track of the total collisional momentum exchange during a long period, and its derivative was obtained by numerical differentiation. The structure factor is obtained through a temporal average of a fast Fourier transform approximation to the discrete Fourier transform of the particle positions $\|\sum_i \exp(-\mathrm{i}\boldsymbol{k}\cdot\boldsymbol{r}_i)\|^2$. The value $S(k = 0)$ is estimated by fitting a parabolic dependence for small k and extrapolating to $k = 0$.

As pointed out earlier, the dimensionless time step $\delta t = D/\sqrt{k_\mathrm{B}T_0/m}$ in the SHSD algorithm should be kept reasonably small, $\delta t \ll \min[1, (\phi\chi)^{-1}]$, in order to faithfully simulate the SHSD fluid. As the time step becomes too large we expect to see deviations from the correspondence with the linear core system and thus a violation of thermodynamic consistency. This is indeed observed in our numerical results, shown in figure 2, where we compare the structure factor at the origin as estimated through the equation of state with that obtained from a direct Fourier transform of the particle positions. We should point out that when discussing thermodynamic consistency one has to define what is meant by the derivative $\mathrm{d}p/\mathrm{d}\phi$. We choose to keep the collisional frequency prefactor χ and the *dimensionless* time step δt constant as we change the density, that is, we study the thermodynamic consistency of a *time-discrete* SHSD

J. Stat. Mech. (2009) P11008

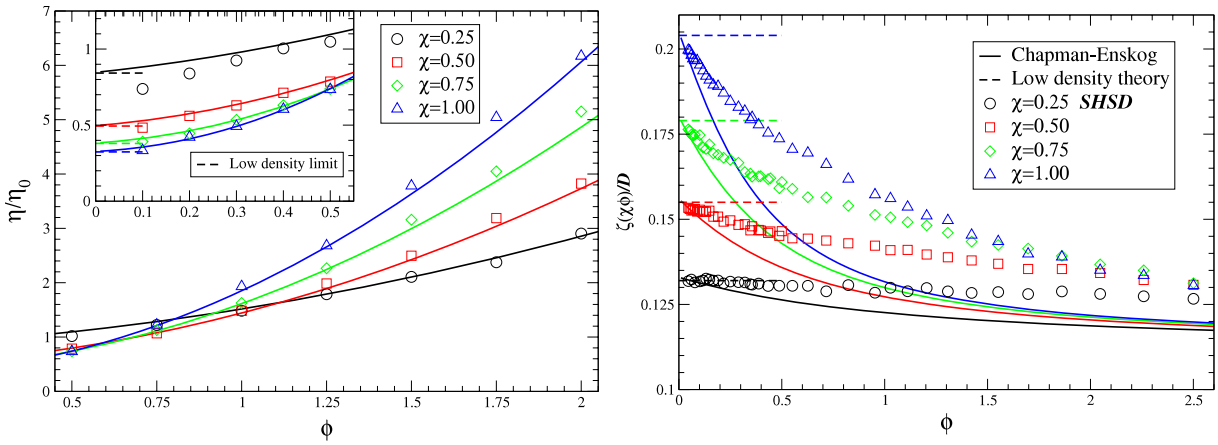

Figure 3. Comparison between numerical results for SHSD at several collision frequencies (different symbols) with predictions based on the stochastic Enskog equation using the HNC approximation for $g_2(x)$ (solid lines). The low density approximations are also indicated (dashed lines). (*Left.*) The normalized shear viscosity η/η_0 at high and low densities (inset), as measured using an externally forced Poiseuille flow. There are significant corrections (Knudsen regime) for large mean free paths (i.e., at low densities and low collision rates). (*Right.*) The normalized diffusion coefficient $\zeta(\chi\phi)/\zeta_0$, as measured from the mean square displacement of the particles. The time step was kept sufficiently small in the SHSD simulations to ensure that the results faithfully represent the SHSD fluid with time step errors smaller than the statistical and measurement errors.

fluid defined by the parameters ϕ, χ *and* δt. The results in figure 2 show that there are significant deviations from thermodynamic consistency when the average number of collisions per particle per time step is larger than 1. This happens at the highest densities for $\delta t \gtrsim 0.1$, but is not a problem at the lowest densities. Nevertheless, a visible inconsistency is observed even at the lower densities for $\delta t \gtrsim 0.25$, which arises because particles travel too far compared to their own size during a time step.

Having established that the HNC closure provides an excellent approximation $g_2^{(\mathrm{HNC})} \approx g_2$ for the pair correlation function of the SHSD fluid, we can obtain estimates for the transport coefficients by calculating the first four moments of $g_2^{(\mathrm{HNC})}(x)$ and substituting them in the results of the Enskog kinetic theory presented in section 2.1.2. In figure 3 we compare the theoretical predictions for the diffusion coefficient ζ and the viscosity η to the ones directly calculated from SHSD particle simulations. We measure ζ directly from the average mean square displacement of the particles. We estimate η by calculating the mean flow rate in Poiseuille parabolic flow between two thermal hard walls due to an applied constant force on the particles[5]. Surprisingly, good agreement is found for the shear viscosity at all densities. Similar matching was observed for the thermal conductivity κ. The corresponding results for the diffusion coefficient show significant ($\sim$25%) deviations for the self-diffusion coefficient at higher densities because of larger corrections due to higher order correlations.

[5] Similar results are obtained by calculating the viscous contributions to the kinetic and collisional stress tensor in non-equilibrium simulations of Couette shear flow. This kind of calculation additionally gives the split in the viscosity between kinetic and collisional contributions.

J. Stat. Mech. (2009) P11008

3.2. Dynamic structure factors

The hydrodynamics of the spontaneous thermal fluctuations in the SHSD fluid is expected to be described by the Landau–Lifshitz Navier–Stokes (LLNS) equations for the fluctuating field $\boldsymbol{U} = (\rho_0 + \delta\rho, \delta v, T_0 + \delta T)$ linearized around a reference equilibrium state $\boldsymbol{U}_0 = (\rho_0, \boldsymbol{v}_0 = \boldsymbol{0}, T_0)$ [36, 37]. For the SHSD fluid the linearized equation of state is

$$P = p(\phi)\frac{Nk_{\mathrm{B}}T}{V} \approx \left(p_0 + \tilde{c}_T^2\frac{\delta\rho}{\rho_0} + p_0\frac{\delta T}{T_0}\right)\rho_0 c_0^2,$$

and there is no internal energy contribution to the energy density,

$$e \approx \frac{3}{2}\frac{Nk_{\mathrm{B}}T}{V} = e_0 + c_v T_0\delta\rho + \rho_0 c_v \delta T,$$

where $p_0 = p(\phi_0)$, $c_0 = k_{\mathrm{B}}T/m$, and $c_v = 3k_{\mathrm{B}}/2m$, giving an adiabatic speed of sound $c_{\mathrm{s}} = \tilde{c}_s c_0$, where $\tilde{c}_s^2 = \tilde{c}_T^2 + 2p^2/3$. Omitting the δs for notational simplicity, for one-dimensional flows the LLNS equations take the form

$$\begin{bmatrix}\partial_t\rho\\ \partial_t v\\ \partial_t T\end{bmatrix} = -\frac{\partial}{\partial x}\begin{bmatrix}\rho_0 v\\ c_T^2\rho_0^{-1}\rho + p_0 c_0^2 T_0^{-1}T\\ p_0 c_0^2 c_v^{-1} v\end{bmatrix} + \frac{\partial}{\partial x}\begin{bmatrix}0\\ \rho_0^{-1}\eta_0 v_x\\ \rho_0^{-1}c_v^{-1}\kappa_0 T_x\end{bmatrix} + \frac{\partial}{\partial x}\begin{bmatrix}0\\ \rho_0^{-1}\sqrt{2\eta_0 k_{\mathrm{B}}T_0}W^{(v)}\\ \rho_0^{-1}c_v^{-1}T_0\sqrt{2\kappa_0 k_{\mathrm{B}}}W^{(T)}\end{bmatrix}, \tag{12}$$

where $W^{(v)}$ and $W^{(T)}$ are independent spatio-temporal white noise Gaussian fields.

By solving these equations in the Fourier wavevector–frequency domain for $\widehat{\boldsymbol{U}}(k,\omega)$ and performing an ensemble average over the fluctuating stresses we can obtain the equilibrium (stationary) spatio-temporal correlations (covariance) of the fluctuating fields. We express these correlations in terms of the 3×3 symmetric positive-definite *hydrodynamic structure factor matrix* $\boldsymbol{S}_{\mathrm{H}}(k,\omega) = \langle\widehat{\boldsymbol{U}}\widehat{\boldsymbol{U}}^{\star}\rangle$ [5]. The *hydrostatic structure factor matrix* $\boldsymbol{S}_{\mathrm{H}}(k)$ is obtained by integrating $\boldsymbol{S}_{\mathrm{H}}(k,\omega)$ over all frequencies,

$$\boldsymbol{S}_{\mathrm{H}}(k) = \begin{bmatrix}\rho_0 c_T^{-2}k_{\mathrm{B}}T_0 & 0 & 0\\ 0 & \rho_0^{-1}k_{\mathrm{B}}T_0 & 0\\ 0 & 0 & \rho_0^{-1}c_v^{-1}k_{\mathrm{B}}T_0^2\end{bmatrix}. \tag{13}$$

We use $\boldsymbol{S}_{\mathrm{H}}(k)$ for an ideal gas (i.e., for $p_0 = 1$, $\tilde{c}_T = 1$) to non-dimensionalize $\boldsymbol{S}_{\mathrm{H}}(k,\omega)$; for example, we express the spatio-temporal cross-correlation between density and velocity through the dimensionless hydrodynamic structure factor

$$S_{\rho,v}(k,\omega) = (\rho_0 c_0^{-2}k_{\mathrm{B}}T_0)^{-1/2}(\rho_0^{-1}k_{\mathrm{B}}T_0)^{-1/2}\langle\hat{\rho}(k,\omega)\hat{v}^{\star}(k,\omega)\rangle.$$

For the non-ideal SHSD fluid the density fluctuations have a spectrum

$$S_{\rho}(k) = (\rho_0 c_0^{-2}k_{\mathrm{B}}T_0)^{-1}\langle\hat{\rho}(k)\hat{\rho}^{\star}(k)\rangle = \tilde{c}_T^{-2},$$

which only captures the small k behavior of the full (particle) structure factor $S(k)$ (see figure 1), as expected of a continuum theory that does not account for the structure of the fluid. Typically only the density–density dynamic structure factor is considered because it is accessible experimentally via light scattering measurements and thus most familiar. However, in order to fully access the validity of the full LLNS system one should examine

J. Stat. Mech. (2009) P11008

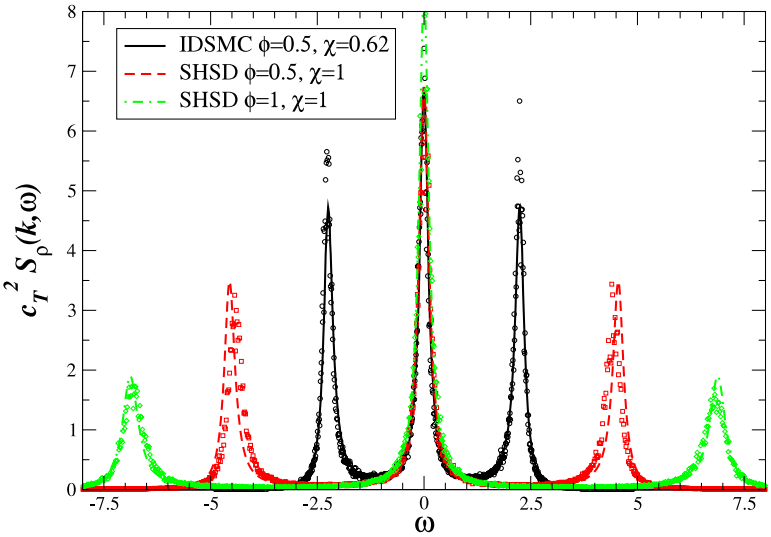

Figure 4. Normalized density fluctuations $\tilde{c}_T^2 S_\rho(k,\omega)$ for $kD \approx 0.070$ for an ideal Maxwell I-DSMC ($\phi = 0.5$, $\chi = 0.62$) and two non-ideal SHSD ($\phi = 0.5$, $\chi = 1$ and $\phi = 1$, $\chi = 1$) fluids of similar kinematic viscosity, as obtained from particle simulations (symbols with parameters, $k_B T_0 = 1$, $m = 1$). The predictions of the LLNS equations are also shown for comparison in the same color (solid lines). For the SHSD fluid we obtained the transport coefficients from the Enskog theory with the HNC approximation to g_2, while for the Maxwell I-DSMC fluid we numerically estimated the viscosity and thermal conductivity.

the dynamic correlations among all pairs of variables. The off-diagonal elements of the static structure factor matrix $\boldsymbol{S}_H(k)$ vanish because the primitive hydrodynamic variables are instantaneously uncorrelated; however, they have non-trivial dynamic correlations visible in the off-diagonal elements of the dynamic structure factor matrix $\boldsymbol{S}_H(k,\omega)$.

In figures 4 and 5 we compare theoretical and numerical results for the hydrodynamic structure factors for the SHSD fluid with $\chi = 1$ at two densities for a small and a medium k value ($kD/(2\pi) \approx 0.01$ and 0.08). In this figure we show selected elements of $\boldsymbol{S}_H(k,\omega)$ as predicted by the analytical solution to equation (12) with parameters obtained by using the HNC approximation to g_2 in the Enskog kinetic theory presented in section 2.1.2. Therefore, for SHSD the theoretical calculations of $\boldsymbol{S}_H(k,\omega)$ do not use any numerical inputs from the particle runs. We also show hydrodynamic structure factors obtained from particle simulations in a quasi-one-dimensional setup in which the simulation cell was periodic and long along the x axis, and divided into 60 hydrodynamic cells of length $5D$. Finite-volume averages of the hydrodynamic conserved variables were then calculated for each cell every ten time steps and a fast Fourier transform used to obtain hydrodynamic structure factors for several wavenumbers. Figure 4 shows very good agreement between theory and numerics, and clearly shows the shifting of the two symmetric Brillouin peaks at $\omega \approx c_s k$ toward higher frequencies as the compressibility of the SHSD fluid is reduced and the speed of sound increased. Figure 5 shows that the positions and widths of the side Brillouin peaks and the width of the central Rayleigh are well predicted for all elements of $\boldsymbol{S}_H(k,\omega)$ for a wide range of k values, demonstrating that the SHSD fluid shows the expected fluctuating hydrodynamic behavior.

J. Stat. Mech. (2009) P11008

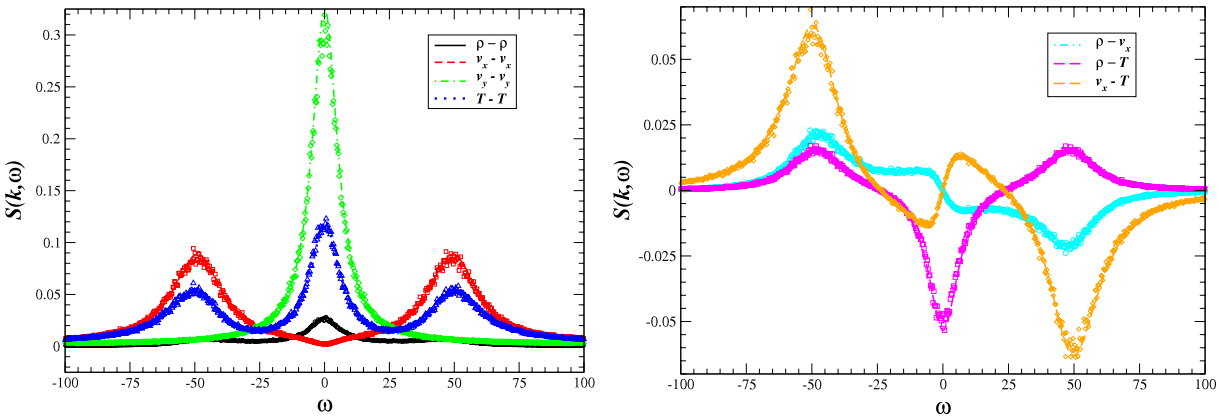

Figure 5. Selected diagonal (left panel) and off-diagonal elements (right panel) of the non-dimensionalized hydrodynamic structure factor matrix $\boldsymbol{S}_{\mathrm{H}}(k,\omega)$ for a large wavenumber $kD \approx 0.50$ for an SHSD fluid at $\phi = 1$, $\chi = 1$ (symbols), compared to the predictions from the LLNS equations (lines of same color). The remaining parameters are as in figure 4.

3.3. Brownian walker VACF

As an illustration of the correct hydrodynamic behavior of the SHSD fluid and the significance of compressibility, we study the velocity autocorrelation function (VACF) $C(t) = \langle v_x(0)v_x(t)\rangle$ for a single neutrally buoyant hard-sphere Brownian bead of mass M and radius R suspended in an SHSD fluid of mass density ρ. This problem is relevant to the modeling of polymer chains or (nano)colloids in solution, and led to the discovery of a long power-law tail in $C(t)$ [38] which has since become a standard test for hydrodynamic behavior of solvents [27, 39, 40]. Here the fluid particles interact via stochastic collisions, exactly as in I-DSMC. The interaction between fluid particles and the bead is treated as if the SHSD particles are hard spheres of diameter D_{s}, chosen to be somewhat smaller than their interaction diameter with other fluid particles (specifically, we use $D_{\mathrm{s}} = D/4$) for computational efficiency reasons, using an event-driven algorithm [41]. Upon collision with the bead the relative velocity of the fluid particle is reversed in order to provide a no-slip condition at the surface of the suspended sphere [40, 41] (slip boundaries give qualitatively identical results). For comparison, an ideal I-DSMC fluid of comparable viscosity is also simulated.

Theoretically, $C(t)$ has been calculated from the linearized (compressible) fluctuating Navier–Stokes (NS) equations [40]. The results are analytically complex even in the Laplace domain; however, at short times an inviscid compressible approximation applies. At large times the compressibility does not play a role and the incompressible NS equations can be used to predict the long-time tail. At short times, $t < t_{\mathrm{c}} = 2R/c_{\mathrm{s}}$, the major effect of compressibility is that sound waves generated by the motion of the suspended particle carry away a fraction of the momentum, so the VACF quickly decays from its initial value $C(0) = k_{\mathrm{B}}T/M$ to $C(t_{\mathrm{c}}) \approx k_{\mathrm{B}}T/M_{\mathrm{eff}}$, where $M_{\mathrm{eff}} = M + 2\pi R^3\rho/3$. At long times, $t > t_{\mathrm{visc}} = 4\rho R_{\mathrm{H}}^2/3\eta$, the VACF decays as in an incompressible fluid, with an asymptotic power-law tail $(k_{\mathrm{B}}T/M)(8\sqrt{3\pi})^{-1}(t/t_{\mathrm{visc}})^{-3/2}$, in disagreement with predictions based on the Langevin equation (Brownian dynamics), $C(t) = (k_{\mathrm{B}}T/M)\exp(-6\pi R_{\mathrm{H}}\eta t/M)$.

J. Stat. Mech. (2009) P11008

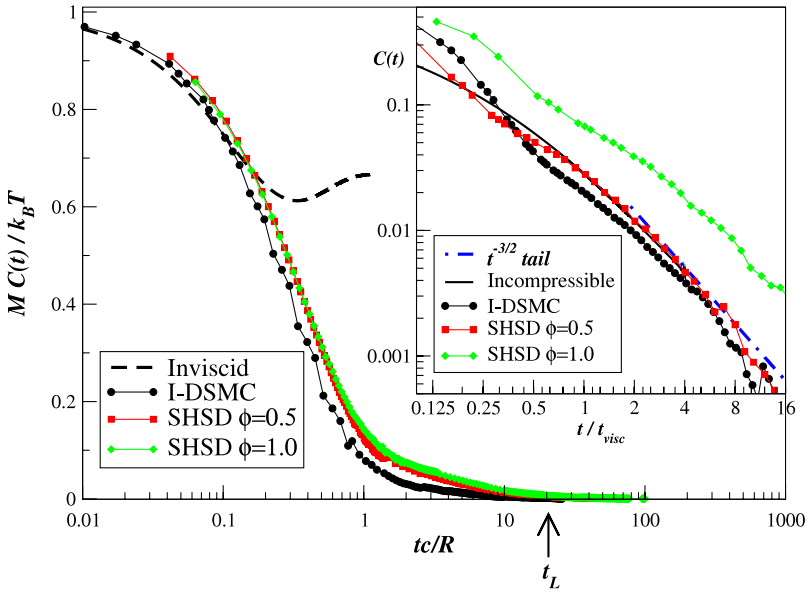

Figure 6. The normalized velocity autocorrelation function for a neutrally buoyant hard-sphere suspended in a non-ideal SHSD ($\chi = 1$) fluid at two densities (symbols), $\phi = 0.5$ and 1.0, as well as an ideal Maxwell I-DSMC fluid ($\phi = 0.5$, $\chi = 0.62$, symbols), at short and long times (inset). For the more compressible (less viscous) fluids the long-time tails are statistically measurable only up to $t/t_{\rm visc} \approx 5$. The theoretical predictions based on the inviscid, for short times, or incompressible, for long times, Navier–Stokes equations are also shown (lines).

We have estimated the effective (hydrodynamic) colloid radius $R_{\rm H}$ from numerical measurements of the Stokes friction force $F = -6\pi R_{\rm H}\eta v$ and found it to be somewhat larger than the hard-core collision radius $R + D_{\rm s}/2$, but for the calculations below we use $R_{\rm H} = R + D_{\rm s}/2$.

In figure 6 numerical results for the VACF in a Maxwell I-DSMC fluid and an SHSD fluid at two different densities are compared to the theoretical predictions. The diameter of the nanocolloidal particle is only $2.5D$ (i.e., $R_{\rm H} = 1.375D$), although we have performed simulations using larger spheres as well with very similar (but less accurate) results. Since periodic boundary conditions were used we only show the tail up to about the time at which sound waves generated by its periodic images reach the particle, $t_L = L/c_{\rm s}$, where the simulation box was $L = 25D$. In dimensionless units, the viscosity $\eta = \tilde{\eta}D^{-2}\sqrt{mk_{\rm B}T}$ was measured to be $\tilde{\eta} \approx 0.75$ for both the Maxwell I-DSMC fluids and the SHSD fluid at $\phi = 0.5$, and $\tilde{\eta} \approx 1.9$ for SHSD at $\phi = 1$. The results in figure 6 are averages over 10 runs, each of length $T/t_{\rm visc} \approx 2 \times 10^5$ for I-DSMC, $T/t_{\rm visc} \approx 1 \times 10^5$ for SHSD at $\phi = 0.5$, and $T/t_{\rm visc} \approx 4.5 \times 10^4$ for SHSD at $\phi = 1.0$, where in atomistic time units $t_0 = D\sqrt{m/k_{\rm B}T}$ the viscous timescale is $t_{\rm visc}/t_0 \approx 6\phi(R_{\rm H}/D)^2/(3\pi\tilde{\eta}) \approx 0.8$.

It is seen, as predicted, that the compressibility or the sound speed $c_{\rm s}$ determines the early decay of the VACF. The exponent of the power-law decay at large times is also in agreement with the hydrodynamic predictions. The coefficient of the VACF tail agrees reasonably well with the hydrodynamic prediction for the less dense fluids; however, there is a significant deviation of the coefficient for the densest fluids, perhaps due to ordering of

J. Stat. Mech. (2009) P11008

the fluid around the suspended sphere, not accounted for in continuum theory. In order to study this discrepancy in further detail one would need to perform simulations with a much larger bead. This is prohibitively expensive with the serial event-driven algorithm used here [41] and requires either parallelizing the code or using a hybrid particle–continuum method [29], which we leave for future work.

4. Conclusions

We have successfully generalized the traditional DSMC algorithm for simulating rare gas flows to flows of dense non-ideal fluids. Constructing such a thermodynamically consistent stochastic hard-sphere dynamics (SHSD) algorithm required first eliminating the grid artifacts from traditional DSMC. These artifacts are small in traditional DSMC simulations of rarefied gases because the collisional cell size is kept significantly smaller than the mean free path [42], but become pronounced when dense flows are simulated because the collisional stress tensor is not isotropic. Our isotropic DSMC (I-DSMC) method is a grid-free DSMC variant with pairwise spherically symmetric *stochastic* interactions between the particles, just as for classical fluids simulated by molecular dynamics (MD) one uses a pairwise spherically symmetric *deterministic* interaction potential. The I-DSMC method can therefore be viewed as a transition from the DSMC method, suitable for rarefied flows, to the MD method, suitable for simulating dense liquids (and solids).

It has long been apparent that manipulating the stochastic collision rules in DSMC can lead to a wide range of fluid models, including non-ideal ones [20, 43]. It has also been realized that DSMC, as a kinetic Monte Carlo method, is not limited to solving the Boltzmann equation [31] but can be generalized to Enskog-like kinetic equations [22, 23]. However, what has been so far elusive is constructing a DSMC collision model that is thermodynamically consistent, meaning that the resulting fluid structure and the equation of state are consistent with each other as required by statistical mechanics. We overcame this hurdle here by constructing stochastic collision kernels in I-DSMC to be as close as possible to those of the classical hard-sphere deterministic system. Thus, in the SHSD algorithm, randomly chosen pairs of approaching and overlapping particles undergo collisions as if they were hard spheres of variable diameter. This is similar to the modified collision rules used to construct a consistent non-ideal multi-particle collision dynamics fluid in [18, 19].

We demonstrated the consistent thermodynamic behavior of the SHSD system by numerically observing that it has identical pair correlations and thermodynamic properties to a Hamiltonian system of penetrable spheres interacting with a linear core potential, even up to solid densities. We found that at fluid densities the pair correlation function $g_2(r)$ of the linear core system is well described by the approximate HNC closure, enabling us to obtain moments of $g_2(r)$. These moments were then used as inputs in a modified Chapman–Enskog calculation to obtain excellent estimates of the equation of state and transport coefficients of the SHSD fluid over a wide range of densities. If our conjecture that the SHSD fluid behaves thermodynamically identically to the linear core fluid is correct, it is important to obtain a better theoretical understanding of the reasons for this surprising relation between a stochastic and a deterministic fluid. Importantly, it is an open question whether by choosing a different collision kernel one can obtain

J. Stat. Mech. (2009) P11008

stochastic fluids corresponding to Hamiltonian systems of penetrable spheres interacting with effective pair potentials $U_{\text{eff}}(r)$ other than the linear core potential.

The SHSD algorithm is similar in nature to DPD and has a similar computational complexity. The essential difference is that DPD has a continuous-time formulation (a system of stochastic ODEs), whereas the SHSD dynamics is discontinuous in time (master equation). This is similar to the difference between MD for continuous potentials and discontinuous potentials. Just as DSMC is a stochastic alternative to hard-sphere MD for low density gases, SHSD is a stochastic modification of hard-sphere MD for dense gases. On the other hand, DPD is a modification of MD for smooth potentials to allow for larger time steps and a conservative thermostat.

A limitation of SHSD is that for reasonable values of the collision frequency ($\chi \sim 1$) and density ($\phi \sim 1$) the fluid is still relatively compressible compared to a dense liquid, $S(k=0) = \tilde{c}_T^{-2} > 0.1$. Indicative of this is that the diffusion coefficient is large relative to the viscosity as it is in typical DPD simulations, so the Schmidt number $S_c = \eta(\rho\zeta)^{-1}$ is less than 10 instead of being on the order of 100–1000. Achieving higher $\tilde{c}_T$ or S_c requires high collision rates (for example, $\chi \sim 10^4$ is used in [32]) and appropriately smaller time steps to ensure that there is at most one collision per particle per time step, and this requires a computational effort similar to that in hard-sphere molecular dynamics at a comparable density. At low and moderate gas densities the SHSD algorithm is not as efficient as DSMC at a comparable collision rate. However, for a wide range of compressibilities, SHSD is several times faster than the alternative deterministic event-driven MD (EDMD) for hard spheres [24, 44]. Furthermore, SHSD has several important advantages over EDMD, in addition to its simplicity:

(1) SHSD has several controllable parameters that can be used to change the transport coefficients and compressibility, notably the usual density ϕ but also the cross-section factor χ and others[6], while EDMD only has density.
(2) SHSD is time driven rather than event driven, thus allowing for easy parallelization.
(3) SHSD can be more easily coupled to continuum hydrodynamic solvers, just like ideal gas DSMC [45] and DPD [46, 47]. Strongly structured particle systems, such as fluids with strong interparticle repulsion (e.g., hard spheres), are more difficult to couple to hydrodynamic solvers [48] than ideal fluids, such as MPCD or (I-)DSMC, or weakly structured fluids, such as DPD or SHSD fluids.

Finally, the stochastic particle model on which SHSD is based is intrinsically interesting, and theoretical results for models of this type will be helpful for the development of consistent particle methods for fluctuating hydrodynamics.

Acknowledgments

The work of A Donev was performed under the auspices of the US Department of Energy at Lawrence Livermore National Laboratory under Contract DE-AC52-07NA27344 (LLNL-JRNL-415281). We thank Ard Louis for sharing his expertise and code for solving the HNC equations for penetrable spheres. We thank Salvatore Torquato, Frank Stillinger, Andres Santos, and Jacek Polewczak for their assistance and advice.

[6] For example, one can combine rejection-free Maxwell collisions with hard-sphere collisions in order to tune the viscosity without affecting the compressibility. The efficiency is significantly enhanced when the fraction of accepted collisions is increased; however, the compressibility is also increased at a comparable collision rate.

J. Stat. Mech. (2009) P11008

References

[1] Squires T M and Quake S R, *Microfluidics: fluid physics at the nanoliter scale*, 2005 *Rev. Mod. Phys.* **77** 977

[2] Hu G and Li D, *Multiscale phenomena in microfluidics and nanofluidics*, 2007 *Chem. Eng. Sci.* **62** 3443

[3] Bell J B, Garcia A and Williams S A, *Numerical methods for the stochastic Landau–Lifshitz Navier–Stokes equations*, 2007 *Phys. Rev.* E **76** 016708

[4] De Fabritiis G, Serrano M, Delgado-Buscalioni R and Coveney P V, *Fluctuating hydrodynamic modeling of fluids at the nanoscale*, 2007 *Phys. Rev.* E **75** 026307

[5] Donev A, Vanden-Eijnden E, Garcia A L and Bell J B, *On the accuracy of explicit finite-volume schemes for fluctuating hydrodynamics*, 2009 arXiv:0906.2425

[6] Kadau K, Rosenblatt C, Barber J L, Germann T C, Huang Z, Carles P and Alder B J, *The importance of fluctuations in fluid mixing*, 2007 *Proc. Nat. Acad. Sci.* **104** 7741

[7] Dünweg B and Ladd A J C, *Lattice Boltzmann simulations of soft matter systems*, 2009 *Adv. Comput. Simulation Approaches for Soft Matter Sci.* III **221** 89

[8] Atzberger P J, Kramer P R and Peskin C S, *A stochastic immersed boundary method for fluid-structure dynamics at microscopic length scales*, 2007 *J. Comput. Phys.* **224** 1255

[9] Aust C, Kroger M and Hess S, *Structure and dynamics of dilute polymer solutions under shear flow via nonequilibrium molecular dynamics*, 1999 *Macromolecules* **32** 5660

[10] Fan X, Phan-Thien N, Chen S, Wu X and Ng T Y, *Simulating flow of DNA suspension using dissipative particle dynamics*, 2006 *Phys. Fluids* **18** 063102

[11] Ripoll M, Mussawisade K, Winkler R G and Gompper G, *Low-Reynolds-number hydrodynamics of complex fluids by multi-particle-collision dynamics*, 2004 *Europhys. Lett.* **68** 106

[12] Lee S H and Kapral R, *Mesoscopic description of solvent effects on polymer dynamics*, 2006 *J. Chem. Phys.* **124** 214901

[13] Noguchi H, Kikuchi N and Gompper G, *Particle-based mesoscale hydrodynamic techniques*, 2007 *Europhys. Lett.* **78** 10005

[14] Donev A, Garcia A L and Alder B J, *Stochastic hard-sphere dynamics for hydrodynamics of non-ideal fluids*, 2008 *Phys. Rev. Lett.* **101** 075902

[15] Alexander F J and Garcia A L, *The direct simulation Monte Carlo method*, 1997 *Comput. Phys.* **11** 588

[16] Luo L-S, *Theory of the lattice Boltzmann method: lattice Boltzmann models for nonideal gases*, 2000 *Phys. Rev.* E **62** 4982

[17] Pagonabarraga I and Frenkel D, *Non-ideal DPD fluids*, 2000 *Mol. Simul.* **25** 167

[18] Ihle T, Tüzel E and Kroll D M, *Consistent particle-based algorithm with a non-ideal equation of state*, 2006 *Europhys. Lett.* **73** 664

[19] Tüzel E, Ihle T and Kroll D M, *Constructing thermodynamically consistent models with a non-ideal equation of state*, 2006 *Math. Comput. Simul.* **72** 232

[20] Alexander F J, Garcia A L and Alder B J, *A consistent Boltzmann algorithm*, 1995 *Phys. Rev. Lett.* **74** 5212

[21] Garcia A L and Wagner W, *The limiting kinetic equation of the consistent Boltzmann algorithm for dense gases*, 2000 *J. Stat. Phys.* **101** 1065

[22] Montanero J M and Santos A, *Simulation of the Enskog equation a la Bird*, 1997 *Phys. Fluids* **9** 2057

[23] Frezzotti A, *A particle scheme for the numerical solution of the Enskog equation*, 1997 *Phys. Fluids* **9** 1329

[24] Alder B J and Wainwright T E, *Studies in molecular dynamics. I. General method*, 1959 *J. Chem. Phys.* **31** 459

[25] Louis A A, Bolhuis P G and Hansen J P, *Mean-field fluid behavior of the Gaussian core model*, 2000 *Phys. Rev.* E **62** 7961

[26] Polewczak J and Stell G, *Transport coefficients in some stochastic models of the revised Enskog equation*, 2002 *J. Stat. Phys.* **109** 569

[27] Ihle T and Kroll D M, *Stochastic rotation dynamics. II. Transport coefficients, numerics, and long-time tails*, 2003 *Phys. Rev.* E **67** 066706

[28] Bird G A, 1994 *Molecular Gas Dynamics and the Direct Simulation of Gas Flows* (Oxford: Clarendon)

[29] Donev A, Bell J B, Garcia A L and Alder B J, *A hybrid particle–continuum method for hydrodynamics of complex fluids*, 2009 arXiv:0910.3968

[30] Wagner W, *A convergence proof for Bird's direct simulation Monte Carlo method for the Boltzmann equation*, 1992 *J. Stat. Phys.* **66** 1011

[31] Brey J J and Cubero D, 2001 *Granular Gases (Lecture Notes in Physics)* Hydrodynamic Transport Coefficients of Granular Gases (Heidelberg: Springer) pp 59–78

J. Stat. Mech. (2009) P11008

[32] Lowe C P, *An alternative approach to dissipative particle dynamics*, 1999 *Europhys. Lett.* **47** 145
[33] Lachowicz M and Pulvirenti M, *A stochastic system of particles modelling the Euler equations*, 1990 *Arch. Ration. Mech. Anal.* **109** 81
[34] Ge W and Li J, *Macro-scale phenomena reproduced in microscopic systems—pseudo-particle modeling of fluidization*, 2003 *Chem. Eng. Sci.* **58** 1565
[35] Mladek B M, Charbonneau P, Likos C N, Frenkel D and Kahl G, *Multiple occupancy crystals formed by purely repulsive soft particles*, 2008 *J. Phys.: Condens. Matter* **20** 494245
[36] Landau L D and Lifshitz E M, 1959 *Fluid Mechanics* vol 6 *Course of Theoretical Physics* (Oxford: Pergamon)
[37] De Zarate J M O and Sengers J V, 2006 *Hydrodynamic Fluctuations in Fluids and Fluid Mixtures* (Oxford: Elsevier Science)
[38] Alder B J and Wainwright T E, *Decay of the velocity autocorrelation function*, 1970 *Phys. Rev.* A **1** 18
[39] Heemels M W, Hagen M H J and Lowe C P, *Simulating solid colloidal particles using the lattice-Boltzmann method*, 2000 *J. Comput. Phys.* **164** 48
[40] Padding J T and Louis A A, *Hydrodynamic interactions and Brownian forces in colloidal suspensions: coarse-graining over time and length scales*, 2006 *Phys. Rev.* E **74** 031402
[41] Donev A, Garcia A L and Alder B J, *Stochastic event-driven molecular dynamics*, 2008 *J. Comput. Phys.* **227** 2644
[42] Alexander F, Garcia A L and Alder B J, *Cell size dependence of transport coefficients in stochastic particle algorithms*, 1998 *Phys. Fluids* **10** 1540
Alexander F, Garcia A L and Alder B J, 2000 *Phys. Fluids* **12** 731 (erratum)
[43] Baras F, Malek Mansour M and Garcia A L, *Microscopic simulation of dilute gases with adjustable transport coefficients*, 1994 *Phys. Rev.* E **49** 3512
[44] Donev A, *Asynchronous event-driven particle algorithms*, 2008 *SIMULATION: Trans. Soc. Modell. Simul. Int.* **85** 229
[45] Williams S A, Bell J B and Garcia A L, *Algorithm refinement for fluctuating hydrodynamics*, 2008 *SIAM Multiscale Model. Simul.* **6** 1256
[46] Delgado-Buscalioni R, Kremer K and Praprotnik M, *Concurrent triple-scale simulation of molecular liquids*, 2008 *J. Chem. Phys.* **128** 114110
[47] Kojic M, Filipovic N and Tsuda A, *A mesoscopic bridging scale method for fluids and coupling dissipative particle dynamics with continuum finite element method*, 2008 *Comput. Methods Appl. Mech. Eng.* **197** 821
[48] Delgado-Buscalioni R and De Fabritiis G, *Embedding molecular dynamics within fluctuating hydrodynamics in multiscale simulations of liquids*, 2007 *Phys. Rev.* E **76** 036709

J. Stat. Mech. (2009) P11008